Wavelength calibration of narrowband ArF laser with iron hollow cathode lamp

Zhijun Yuan (袁志军)[1,2], Haibo Zhang (张海波)[1,2], Ren Ye (叶 韧)[1,2], Jun Zhou (周 军)[1,2,*], Yunrong Wei (魏运荣)[1,2], and Qihong Lou (楼祺洪)[1,2]

[1]*Shanghai Institute of Optics and Fine Mechanics, Chinese Academy of Sciences, Shanghai 201800, China*

[2]*Shanghai Key Laboratory of All Solid-state Laser and Applied Techniques, Shanghai 201800, China*

**Corresponding author: junzhousd@siom.ac.cn*

Received December 5, 2016; accepted March 30, 2017; posted online April 20, 2017

Accurate and precise wavelength controlling of narrowband excimer lasers is essential for the lithography of an integrated circuit. High-precision wavelength tuning and calibration of a line-narrowed ArF laser are presented in this work. The laser spectrum is narrowed to a sub-picometer with a line narrowing system. Absolute wavelength calibration of the line-narrowed laser is performed based on the optogalvanic (OG) effect using iron hollow cathode discharge (HCD). An sccuracy of better than 0.1 pm for wavelength tuning and calibration is achieved with our homemade wavemeter.

OCIS codes: 140.2180, 150.1488, 300.6440, 300.3700, 110.5220.

doi: 10.3788/COL201715.071402.

ArF lasers emitting around 193 nm are widely used for photolithographic processing of integrated circuit devices[1]. This kind of laser should provide a narrow spectral band around a precisely determined and finely adjustable absolute wavelength. The deviation of the wavelength may result in the linewidth broadening and the defocus on the exposure plane[1]. Therefore, it is desirable to calibrate the wavelength of the ArF lasers within a range of ± 0.05 pm[2]. Wavelength calibrations of the laser source for lithography also require a compact wavemeter with sub-picometer precision. Researches on high-precision spectrum detection[2–6] in the ultraviolet (UV) region have been extensively studied in recent years.

The optogalvanic (OG) effect described by Babin *et al.*[7,8] permits a very precise and reliable determination of an absolute emission wavelength for an excimer laser system. When the line-narrowed laser beam is incident into a see-through hollow cathode discharge (HCD) lamp, the OG effect originates from a change in the impedance in a steady-state glow discharge when the discharge medium resonantly absorbs laser photons[9]. Consequently, the photodetector behind the HCD lamp can observe an intensity drop of laser energy around the wavelength of absorption. This effect has been shown to be a powerful and inexpensive technique for laser stabilization or wavelength calibration[10,11], especially in a lithography application[2,7,12]. For example, emission lines of a platinum HCD lamp at 193.22433 and 193.43690 nm (vacuum wavelength) have been used for the calibration of an ArF laser[12]. Nevertheless, very few researches on ArF laser wavelength calibration with an iron lamp have been reported so far. Moreover, the laser power incident into the HCD has to be very carefully controlled for the ArF laser source because the OG signal amplitude tends to saturation at relatively high laser energy[13]. On the other hand, the ArF laser energy around 193.22433 nm is relatively low due to the oxygen absorption; accordingly, a high signal-to-noise ratio (SNR) OG signal around the absorption wavelength is hardly accessible.

Because the OG signal is vulnerable to the interference from the surrounding electromagnetic field, many researchers since the 19th century have used the boxcar averager[8] or lock-in amplifier[14] to get a high SNR signal. However, the bulky and complicated structure of the boxcar averager or lock-in amplifier prevents its integration in an optical lithography machine.

In our experiment, the wavelength of the ArF laser was calibrated by measuring the OG voltage directly. Relatively high SNR absorption for absolute wavelength calibration was obtained. The ArF laser was line-narrowed below 0.4 pm by a line narrowing system. Furthermore, high-precision laser wavelength tuning and real-time measurements with a homemade wavemeter were also demonstrated in this work.

Before the wavelength calibration process, the broadband emission spectrum of nearly 500 pm of the ArF laser spectrum has to be narrowed to the sub-picometer scale. The narrow spectrum is obtained by an EX100 excimer laser (provided by GAM LASER-INC, maximum pulse energy of 20 mJ and repetition of 500 Hz) coupled with a line narrowing system, which consists of three CaF_2 prisms and a grating. In order to reduce the energy loss in the beam path, the prisms and grating are equipped in a sealed cavity purged with nitrogen. The design and setup of the line narrowing system can be found in our early works[15–17]. The bandwidth (full width at half-maximum, FWHM) of the narrowband laser is about 0.38 pm, and the maximum pulse energy is 0.5 mJ. Figure 1 shows the typical laser spectrum recorded by a spectrometer (provided by LTB Lasertechnik Berlin, model ELIAS III, resolution of 0.022 pm for the linewidth, absolute accuracy of ± 5 pm for wavelength calibration).

 © 2017 Chinese Optics Letters

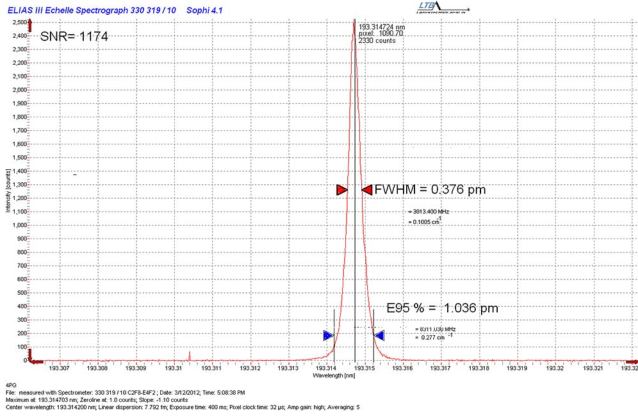

Fig. 1. Spectrum of the line-narrowed ArF laser (FWHM 0.376 pm).

Smooth scanning of the laser wavelength is accomplished by rotating the grating with a precision of 1×10^{-5} deg/step.

The schematic diagram of the wavelength calibration is shown in Fig. 2. The narrowband tunable laser is split into two beams, which are designed to realize the wavelength measurement and calibration, respectively.

One portion of the laser beam is focused to a spot radius of approximately 0.5 mm inside the center hole of the HCD lamp. Then, it is guided into the spectrometer (ELIAS III, LTB), which is used to measure the linewidth and to acquire the approximate value of the wavelength.

The OG detector in this work is a see-through hollow cathode iron lamp (Hamamatsu L2783 series laser galvatron) filled with xenon and Ne gas and supplied by a high-voltage direct current (DC) power ranging from 0 to 1000 V (provided by KIKUSUI, model PAD1K-0.2L, Ripple Voltage of 500 μV). Its operation circuit, surrounded by dashed lines shown in Fig. 2, consisting of a resistor R of 40 Ω and a capacitor C of 0.047 μF, is packed in a shield case to exclude the external electromagnetic induction. The real-time OG signal acquisition and processing is accomplished by a high-speed data acquisition card (provided by Advantech, model PCI-1714).

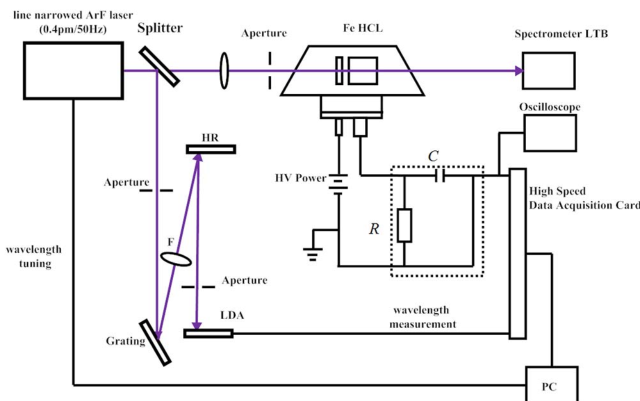

Fig. 2. Experimental setup for wavelength calibration of the ArF laser. HCL, hollow cathode lamp; HV, high voltage; PC personal computer; HR, high-reflection mirror.

The waveform of the OG signal was also presented in a digital storage oscilloscope for observation.

The other portion of the narrow-lined laser incident to an echelle grating (Newport, 112.96 g/mm, 79° blaze angle), and the diffractive beam was focused into a linear diode array (LDA). Two 1.0 mm radius apertures are added to prevent the stray light and minimize the spot size[18]. One was added between the beam splitter and the grating, and the other was between the grating and the LDA. The focused spot is about 100 μm, covering 3–4 pixels (FWHM) in the LDA. All of the wavelength measurements in this work are performed in the air.

At first, the precision of the wavelength tuning and measurement will be examined and analyzed here. The minimum incremental motion and repeatability of the linear motor is 0.1 μm, yielding about a 0.03 pm precision for wavelength tuning. As depicted in Fig. 2, the wavelength is measured by a diffraction grating in near-Littrow configuration. The high-order diffracted beam is focused and reflected back to the LDA. Based on the diffraction grating equation below,

$$k\lambda = 2d \sin \theta, \tag{1}$$

$$\Delta\lambda = \frac{2d \cos \theta}{k} \Delta\theta, \tag{2}$$

where k is the diffraction order, λ is the laser wavelength, d is the distance between groves, and θ is the diffraction angle. With the angle $\Delta\theta$ in Eq. (2) measured by position change of the laser spot on the LDA ΔL and the focal length f,

$$\Delta\theta = \frac{\Delta L}{f}. \tag{3}$$

The value of $\Delta\lambda$ can be expressed as follows:

$$\Delta\lambda = \frac{2d \cos \theta \cdot \Delta L}{k \cdot f}. \tag{4}$$

According to Eq. (4), gratings with a higher diffraction order and groove density can be conducive to the improvement of the resolution. Furthermore, a lens with a longer focal length is also desirable for the wavelength measurement. The key parameters of the wavelength measurement are listed in Table 1.

From Eq. (4), the wavelength can change linearly with the position of the laser spot on the LDA ΔL. Figure 3 shows the pixel position of laser spot on the LDA and the corresponding wavelength in the range of 193.1–193.5 nm. The wavelength data are roughly measured with the spectrometer (ELIAS III, LTB). The two columns of data presented in Fig. 3 shows a good linear relationship. The value of wavelength λ is determined by the pixel position of the laser spot on the LDA, shown as the equation below,

Table 1. Key Parameters of the Wavelength Measurement

Parameters	Values
Diffraction order of the grating k	90
Distance between groves d (mm)	1/112.96
Diffraction angle of the grating θ (deg.)	79
Pixel length (μm)	25
Focal length f (mm)	200

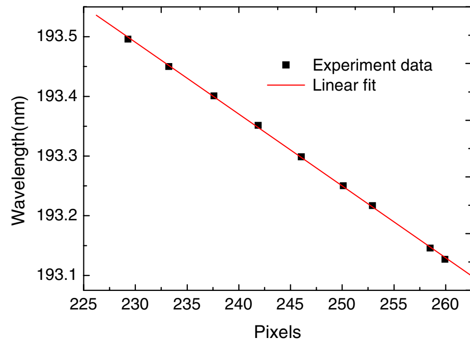

Fig. 3. Wavelength with the position of the laser spot on the LDA.

$$\lambda = (-0.0120357 \text{ nm/pixel}) * P + 196.25883. \quad (5)$$

By fitting a Gaussian curve to the data of the laser spot on the LDA, which represents the laser wavelength, the precision for the wavelength measurement is improved. The long-term (60 s) wavelength measurement with our wavemeter shows that the variation of the measured wavelength is within 0.06 pm at a steady state.

The wavemeter can now tune and measure the wavelength with adequate precision, yet it is far from accurate because the absolute accuracy of the spectrometer (ELIAS, LTB) is about ±5 pm. Therefore, the wavemeter needs to be calibrated with the hollow cathode lamp.

Next, the effect of laser energy and discharge current on the OG signal amplitude at different wavelengths is studied.

The observed transient waveform of the OG signal by an oscilloscope is shown in Fig. 4. The OG signal is composed of a fast rising peak followed by an exponential decay to the signal with an opposite sign, which then returns to the base line. It usually lasts 20–40 μs, and its waveform and lasting time depends on the discharge conditions, such as the energy level of the atoms and plasma relaxation[19]. Mahmood *et al.*[20] have simulated the time-resolved OG signal by the sum of two exponential attenuation functions. The time-resolve of such an OG signal can be composed by two parts[21]: a pure neon part and the penning part. The pure neon part consists of a negative pulse and a positive pulse in the first tens of microseconds, it is commonly observed in neon HCD, while the penning part often occurs after a diffusion time interval of about 30 μs, It is related to the metal atom ionization and the transition of the neon atom from the metastable level to the ground level.

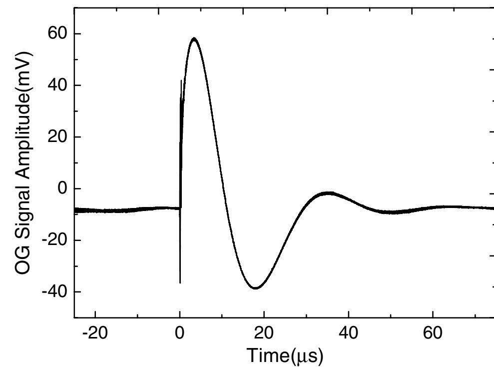

Fig. 4. Waveform of iron OG signal recorded by an oscilloscope.

When the laser wavelength approaches the absorption wavelength of the Fe element (193.38978 nm in our case), the ionized Fe atoms will participate in collisions with laser-excited neon atoms in the excited state. Then, the penning ionization process becomes stronger when laser irradiation excites the Fe atoms from the $3d^6 4s^2$ to the $3d^6 4s^5 p$ level at this resonant absorption state. The more detailed investigation on the penning–ionization interaction between the cathode element and neon by the energy level diagram is shown in Refs. [22,23]. Here, we mainly focus on the change of the OG signal amplitude during the wavelength scanning because it is crucial for the wavelength calibration. The amplitude of the OG signal is observed ranging from 20 mV to over 100 mV, depending on the laser energy, discharge current, and laser wavelength.

From the National Institute of Standards and Technology (NIST) atomic spectrum database, there are two absorption lines in the UV region for the Fe element, which are 193.45350 and 193.72683 nm in the vacuum, and 193.38978 and 193.66307 nm in the air. Due to the fact that the emission spectrum of the ArF laser is from 193.0 to 193.5 nm, the emission line of 193.38978 nm (in the air) is chosen for the ArF laser wavelength calibration in this work.

The relationship between the OG intensity and discharge current at different wavelengths of 193.38978 and 193.38600 nm is depicted in Fig. 5. The two wavelengths correspond to the resonant absorption (NIST) and non-resonant absorption state of the iron lamp, respectively. The OG signal amplitude is found to drop considerably at 193.38600 nm, while it remains almost constant with the discharge current at 193.38978 nm. The possible reason is because the OG signal amplitude for the metal cathode, which contributes to the penning part, increases dramatically with the current at the resonant absorption state. This effect has been observed by Saini *et al.*[21], and they found the peak-to-peak OG signal of europium almost tripled at the europium resonant state

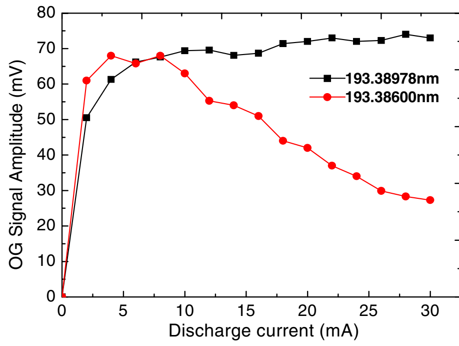

Fig. 5. OG signal amplitude with discharge current.

when the current increased from 7.6 to 13.6 mA. The increasing part derived from the metal cathode may compensate for the decreasing pure neon part at a high current. The experimental results in Fig. 5 mean that, the OG signal amplitude may become stronger at the resonant absorption state during the wavelength scanning process. It can be concluded that wavelength calibration should be performed at a relatively higher discharge current to get a high SNR absorption.

The OG signal amplitude for a different laser energy and discharge current is shown in Fig. 6. It is found that the OG signal amplitude increases almost linearly with laser energy. However, the saturation effect at higher laser intensities, observed by other researchers[13], does not appear in this experiment. The possible reason is that the laser energy is not high enough for saturation. The maximum laser pulse energy is 0.5 mJ, and the portion of that incident into the HCD is less than 0.25 mJ, where most of the laser photons inside the HCD lamp may be absorbed in the glow discharge process.

Lastly, the wavelength calibration is performed by recording the OG signal amplitude while scanning the wavelength in the range of 10 pm. The wavelength scanning range is set from 193.38500 to 193.39500 nm, in order to cover the wavelength of 193.38978 nm. The wavelength scanning and measurement are performed by the wavemeter depicted in Fig. 1. The discharge current is set to be 30 mA, and the laser repetition rate is 50 Hz. The speed of the linear motor is 0.5 μm/s, and the wavelength scan speed is about 0.15 pm/s, so the scanning range from 193.38500 to 193.39500 nm needs 67 s, and the wavelength calibration process can be accomplished in 90 s.

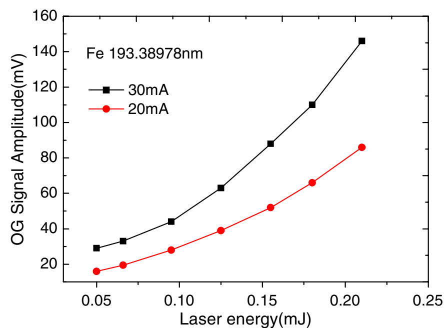

Fig. 6. OG signal amplitude at a different laser power and discharge current.

The experiments have been repeated several times. Four samples of the wavelength scanning data are shown In Fig. 7.

The OG signal amplitude is found to substantially increase, while the laser is resonant with the absorbed wavelength of the Fe atom (193.38978 nm), and high SNR absorption lines are observed during the wavelength scanning. The typical bandwidth (FWHM) of the absorption line is about 1.5 pm. The broadening of the spectral lines may mainly result from the Doppler effect[24], which is caused by the random movements of the particles excited by the discharge and is based on the following equation[25]: $\Delta\lambda = 2\lambda_0\sqrt{2\ln 2\frac{kT}{m_0 c^2}}$, where λ_0 is the wavelength (m) at the center of the absorption line, k is the Boltzmann constant (J/K), m_0 is the atomic mass (kg), c is the speed of light (m/s), T (K) is the excitation temperature (9600 K for the iron HCD lamp[26]), and the broadening linewidth caused by the Doppler effect is estimated to be 1.75 pm, which is close to the observed linewidth (1.5 pm). The minor difference may result from the value of the excitation temperature T (K), which depends on various conditions, such as discharge current and gas pressure. The temperature in this work may be slightly lower than the reported 9600 K in Ref. [26].

The absorption wavelengths corresponding to the OG signal peaks in Fig. 7 are 193.38969, 193.38971, 193.38973, and 193.38979 nm, respectively. It can be seen that the baseline has a strong fluctuation, which may originate from the instability of laser energy. The nominal pulse to pulse stability of the laser is about 2%, but after line narrowing it becomes much worse and is nearly 10%. The pulse energy fluctuation may influence the line center of the OG peak and result in the accuracy reduction. The OG spectrum with a better SNR can be expected if the laser stability is improved.

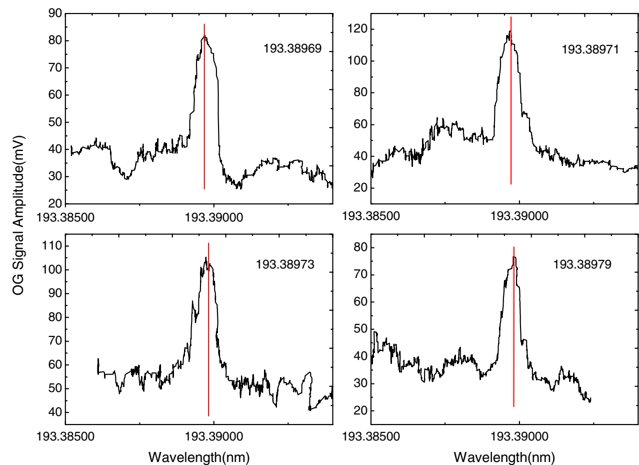

Fig. 7. OG signal amplitude recorded in the wavelength range of 193.38500–193.39500 nm.

Further scanning results show that the accuracy of wavelength calibration is within ±0.1 pm. It is worth pointing out that every time the wavelength scanning is deliberately started slightly different from 193.38500 nm. However, the absorption peaks are found to be exactly around 193.38978 nm. That means the OG signal peaks in Fig. 7 agree well with the absolute spectral line of the Fe element. Then, the wavelength calibration can be accomplished simply by modifying the constant in Eq. (5). Our future work is devoted to wavelength stabilization and to improve spectral resolution.

In conclusion, the OG effect of an iron hollow cathode lamp is investigated experimentally. The results show that the OG signal amplitude at a resonant absorption state increases almost linearly with laser energy and remains constant with the discharge current, while the OG signal amplitude at the non-resonant absorption state decrease dramatically with the discharge current. By detecting the OG signal amplitude directly from iron lamp, we build a high-precision wavelength calibration system. The wavelength accuracy of better than 0.1 pm is achieved in a repeated calibration process.

This work was supported by the National Science and Technology Major Project (No. 2013ZX02202003), the National Key Research and Development Program (No. 2016YFB0402201), K. C. Wong Education Foundation, the Program of Shanghai Technology Research Leader (No. 17XD1424800), the Shanghai Sailing Program of Talented Youth in Science and Technology (No. 17YF1421200), the Key Technologies R&D Program of Jiangsu (Nos. BE2014001 and BE2016005-4), the Natural Science Foundation of Shanghai (Nos. 16ZR1440100 and 16ZR1440200), and the NSAF Foundation of National Natural Science Foundation of China (Nos. U1330134 and 61405202).

References

1. P. Das and R. L. Sandstrom, Proc. IEEE **90**, 1637 (2002).
2. L. Peter and T. Schroeder, "Absolute wavelength calibration of lithography laser using multiple element or tandem see through hollow cathode lamp," U.S. patent US6580517 (June 17, 2003).
3. Y. Wu, Y. Fan, G. Liu, and Y. Zhou, Laser Optoelectron. Progress **52**, 073002 (2015).
4. Y. Fan, Y. Zhou, G. Liu, X. Song, Y. Shan, Q. Wang, and J. Zhao, Chin. J. Lasers **43**, 0202001 (2016).
5. T. Suzuki, H. Kubo, T. Suganuma, T. Yamashita, O. Wakabayashi, and H. Mizoguchi, Proc. SPIE **4000**, 1452 (2001).
6. C. J. D. Jong, A. Lajevardipour, M. Gecevičius, M. Beresna, G. Gervinskas, P. G. Kazansky, Y. Bellouard, A. H. A. Clayton, and S. Juodkazis, Photon. Res. **3**, 283 (2015).
7. F. Babin, P. Camus, J. M. Gagné, P. Pillet, and J. Boulmer, Opt. Lett. **12**, 468 (1987).
8. S. Levesque, F. Babin, and J. M. Gagne, IEEE Trans. Instrum. Meas. **42**, 251 (1993).
9. L. Matsuoka, K. Ogawa, and K. Yokoyama, in *Lasers Electro-Opt. Pacific Rim* (2013), p. 1011.
10. A. R. Victor, M. G. Destro, M. E. Sbampato, J. W. Neri, C. A. B. Silveira, and A. C. Oliveira, Spectrochim. Acta Part B: At. Spectrosc. **66**, 748 (2011).
11. T. L. Chen, C. Y. Lin, J. T. Shy, and Y. W. Liu, J. Opt. Soc. Am. B **30**, 2966 (2013).
12. K. Suzuki and B. W. Smith, *Microlithography Science and Technology*, 2nd ed. (CRC Press, 2007), p. 272.
13. M. N. Reddy, Def. Sci. J. **44**, 279 (1994).
14. I. Siddiqui, S. Khan, B. Gamper, J. Dembczyński, and L. Windholz, J. Phys. B: At. Mol. Opt. Phys. **46**, 065002 (2013).
15. H. Zhang, Z. Yuan, J. Zhou, and Q. Lou, Chin. Opt. Lett. **11**, 041405 (2013).
16. H. Zhang, Z. Yuan, J. Zhou, J. Dong, Y. Wei, and Q. Lou, Chin. J. Lasers **38**, 1102008 (2011).
17. Y. Shan, J. Zhao, H. Li, Q. Wang, P. Sha, Y. Zhou, J. Zhou, Z. Yuan, H. Zhang, and Q. Lou, Chin. J. Lasers **40**, 0402008 (2013).
18. Q. Zhou, J. Pang, X. Li, N. Kai, and R. Tian, Chin. Opt. Lett. **13**, 110501 (2015).
19. M. Blosser, X. L. Han, R. F. Garcia-Sanchez, and P. Misra, Appl. Spectrosc. Sci. Nanomater. **2**, 21 (2015).
20. S. Mahmood, M. Anwar-Ul-Haq, M. Riaz, and M. A. Baig, Eur. Phys. J. D **36**, 1 (2005).
21. V. K. Saini, P. Kumar, S. K. Dixit, and S. V. Nakhe, Appl. Opt. **53**, 4320 (2014).
22. X. Zhu, A. H. Nur, and P. Misra, J. Quantum Spectrosc. Radiat. Transfer **52**, 167 (1994).
23. V. K. Saini, P. Kumar, S. K. Dixit, and S. V. Nakhe, Appl. Opt. **54**, 595 (2015).
24. C. Li, L. Liu, X. Qiu, J. Wei, L. Deng, and Y. Chen, Chin. Opt. Lett. **13**, 013001 (2015).
25. I. B. Gornushkin, L. A. King, B. W. Smith, N. Omenetto, and J. D. Winefordner, Spectrochim. Acta Part B: At. Spectrosc. **54**, 1207 (1999).
26. D. M. Mehs and T. M. Niemczyk, Appl. Spectrosc. **32**, 269 (1978).